Imperfect Digital Fibre Optic Link Based Cooperative Distributed Antennas with Fractional Frequency Reuse in Multicell Multiuser Networks

Xinyi Xu, Rong Zhang, *Member, IEEE,* Salman Ghafoor and Lajos Hanzo, *Fellow, IEEE*

***Abstract*— The achievable throughput of the entire cellular area is investigated, when employing fractional frequency reuse techniques in conjunction with realistically modelled imperfect optical fibre aided distributed antenna systems (DAS) operating in a multicell multiuser scenario. Given a fixed total transmit power, a substantial improvement of the cell-edge area's throughput can be achieved without reducing the cell-centre's throughput. The cell-edge's throughput supported in the worst-case direction is significantly enhanced by the cooperative linear transmit processing technique advocated. Explicitly, a cell-edge throughput of $\eta = 5$ bits/s/Hz may be maintained for an imperfect optical fibre model, regardless of the specific geographic distribution of the users.**

I. Introduction

The classic Unity Frequency Reuse (UFR) pattern may be applied by wireless systems in order to maximize the attainable area spectral efficiency at the cost of increasing the Co-channel Interference (CCI) level, hence the UFR typically exhibits a low throughput at the cell-edge. As a remedy, the Fractional Frequency Reuse (FFR) [1] philosophy may be invoked, which reduced the CCI at the cell-edge at the cost of a reduced area-spectral-efficiency. Hence the FFR scheme is capable of improving the cell-edge Signal-to-Interference-plus-Noise-Ratio (SINR) [2]. As a result, FFR has also been adopted in the Third Generation Partnership Project's (3GPP) Long Term Evolution (LTE) initiative [3] and in the Worldwide interoperability for Microwave Access (WiMAX) [4] system.

By contrast, a DAS improves the cell-edge throughput by placing the Remote Antennas (RA) more close to the cell-edge terminals, hence naturally reducing the pathloss [5]. However, the reduced pathloss will increase the interference imposed on the cell-edge terminals served by the neighbouring RAs. In practice only those MSs can be granted a high throughput, which roam in the vicinity of the RA. When the MS is roaming near the angle halfway between two adjacent RAs [6] [7], its throughput is reduced, hence we will refer to this as the 'worst-case direction' problem. As a potential remedy, cooperative processing techniques which have been considered for Base Stations (BS) [2] [8] may be adopted for the DAS scenario considered in order to mitigate the Inter-RA-Interference (IRI), especially in the worst-case direction. The family of BS cooperation techniques is capable of efficiently mitigating the CCI, hence it was also considered as a candidate for next generation wireless networks by the 3GPP organization [9]. However, the family of BS cooperation techniques still relies on the classic architecture of a single centralized BS covering the entire cell, where the pathloss-and shadow-fading induced problem of the cell-edge users may not be readily solved. Hence, in order to achieve a high throughput for the entire cellular area, especially for the cell-edge terminals, we propose to combine DASs with cooperative BS processing techniques.

For the practical application of DASs, the connection between the BS and RAs may be a coaxial cable, optical fibre or a Radio Rrequency (RF) link [10] [11]. The Radio over Fibre (RoF) [12] and Digital Fibre Optical (DFO) link [13] based transmission technique may also be used for the BS to RA links, which is more reliable than a wireless backhaul, albeit it is also more costly. In contrast to the RoF family [14], the DFO link is immune to the sideband cancellation phenomenon, which occurs in the RoF system [15] [16] and it is capable of avoiding both the inter-modulation distortions of the optical fibre as well as the nonlinearity imposed by the optical components, but this is typically achieved at an increased complexity and cost [13]. Additionally, optical multilevel signalling transmission techniques [17] [18] may be applied for the DFO link, which are capable of reducing the complexity of the optical receiver at the RA. Hence in this study we opted for the DFO link. As a further benefit, DFO techniques also allow us to preprocess the DownLink (DL) transmit signal for all the users in the central BS, before it is transmitted to the mobile station (MS). Hence the DFO backhaul may also support the extension of BS cooperation techniques [19] to DASs. Furthermore, when aiming for supporting Gigabit-transmissions, which is the goal of LTE-Advanced (LTE Release 10) [20], these high-rate systems may suffer from the effects of both the dispersion and nonlinearty imposed by the optical fibre links of the DASs [21]. Hence jointly considering the effects of DFO link and wireless links becomes important, when analyzing the performance of DAS systems designed for LTE-Advanced applications.

Against this background, in this paper *we quantify the*

Acknowledgements: The financial support of the EPSRC under the auspice of the UK-India Advanced Technology Centre in Wireless Communications as well as that of the EU under the auspices of optimix project and of the UK/China scholarships for excellence programme is gratefully acknowledged.

X. Xu is with School of Electronics and Computer Science, University of Southampton, SO17 1BJ Southampton, U.K., and also with School of Electronic Information, Wuhan University, Wuhan, 430072, China (e-mail: xx08r@ecs.soton.ac.uk).

R. Zhang, S. Ghafoor and L. Hanzo are with the School of Electronics and Computer Science, University of Southampton, SO17 1BJ Southampton, U.K. (e-mail: rz@ecs.soton.ac.uk;sag1z07@ecs.soton.ac.uk;lh@ecs.soton.ac.uk).

attainable throughput across the entire cellular coverage area in a multicell, multiuser scenario, when employing cooperative techniques beneficially combined both with realistically modelled imperfect optical fibre aided DASs as well as with FFR. More explicity, we introduced the Split-Step Fourier (SSF) method [22] to analyse how the dispersion and nonlinearity of the optical fibre link affect the throughput of the cell-edge area.

1) Although the dispersion of the optical signalling pulse may be viewed as an undesirable imperfection of a pure optical fibre system, ironically, it might result in beneficial throughput enhancements in the cell-edge area of the non-cooperative RA aided FFR system. This is because the dispersion-induced attenuation of the optical signalling pulses may be capable of mitigating the IRI in the multicell, multiuser scenario. However, we will demonstrate that due to the worst-case direction problem caused by the IRI, the non-cooperative RA aided FFR system may not always lead to an improved attainable throughput in the entire cell-edge area.
2) We will also demonstrate that employing a single omni-directional transmit antenna at each RA and a single receive antenna at each MS, but jointly designing the Transmit PreProcessing (TPP) matrix of all the cooperative RAs combined with FFR is capable of achieving an increased throughput for the entire cell-edge area, regardless of the specific geographic distribution of the users. Furthermore, even though conventional cooperative signal processing techniques are unable to directly mitigate the optical fibre receiver's self-inflicted noise, the proposed cooperative RA-aided FFR system exhibits a higher attainable throughput than conventional non-cooperative FFR aided systems, especially in the worst-case direction.

Our results not included here for reasons of space economy suggest that the IRI experienced in the local cell dominates the interference experienced in the DFO link aided DAS combined with FFR. We also found that the DAS combined with FFR requires a reduced transmit power at each RA, which naturally limits the IRI imposed by the cells using the same frequency band in a tier-two cell. Hence, the IRI inflicted by the tier-two cells will be neglected to simplify our analysis in the multicell multiuser scenario considered.

Our paper is organised as follows. In Section II we introduce the multicell multiuser topology considered, describe the imperfect optical fibre model. In Section III, we outline the received signal model of the non-cooperative DAS with FFR system (Section III-A), introduce several cooperative linear processing techniques (Section III-B) and present our link level results recorded for a range of practical modulation and coding schemes (Section III-C) followed by our performance evaluations in Section IV. Finally, we conclude our discourse in Section V.

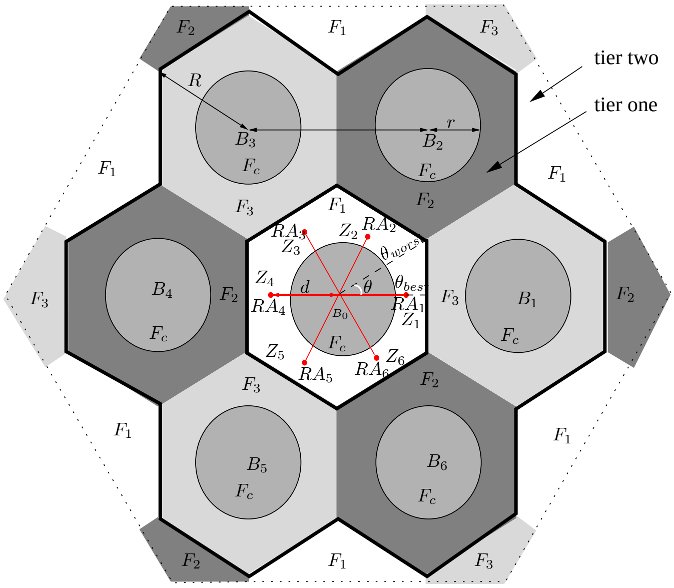

Fig. 1. The toplogy of two tiers of nineteen cells relying on a FFR and DAS arrangement, where $N_r = 6$ RAs are employed. The structure of the cells in tier two is the same as the ones in tier one.

II. System Description and Optical Fibre Modelling

A. Multicell Multiuser System Topology

The multicell multiuser scenario based on the FFR scheme is illustrated in Fig. 1, which consists of two tiers of nineteen hexagonal cells [23] surrounding the central BS B_0, where B_0 is assumed to be at the origin. We assume *symmetry*, where every cell has the same system configuration and focus our attention on cell B_0 of Fig. 1 without any loss of generality. The frequency partitioning strategy of the total available bandwidth F is characterzed by $F_c \cap F_e = \oslash$, where F_c and F_e represent the cell-centre's frequency band and the cell-edge's frequency band, respectively. F_e is divided into three orthogonal frequency bands $F_i, i \in [1, 3]$, exclusively used at the cell-edge of one of the three adjacent cells.

To simplify the structure, we assume that the number of active MSs N_m and RAs N_r is the same ($N_m = N_r$), which implies that each RA may support a single MS. The users are assumed to be randomly distributed in the cell-edge area, and a total of N_m MSs are roaming at any point Z_i, as described by the polar coordinates of $[\theta_{Zi}, L_{Zi}], i \in [1, N_m]$. A total of N_r RAs are employed in each cell described by its polar coordinates denoted by $[\theta_{Ri}, L_{Ri}] = [2\pi(i-1)/N_r, d], i \in [1, N_r]$. Likewise, the BSs in tier-one are described by their polar coordinates of $[\theta_{Bj}, L_{Bj}] = [2\pi(j-1)/6, \sqrt{3}R], j \in [1, 6]$ and the polar coordinates of the BSs in tier-two may also be readily obtained from the underlying simple geometry. Fig. 2 shows a single optical fibre link spanning from the BS to the RA.

B. Imperfect Optical Fibre Model

In order to investigate the system topology introduced above, we assume that the links from BS B_0 of Fig. 1 to the RAs are constituted by a realistic imperfect optical fibre,

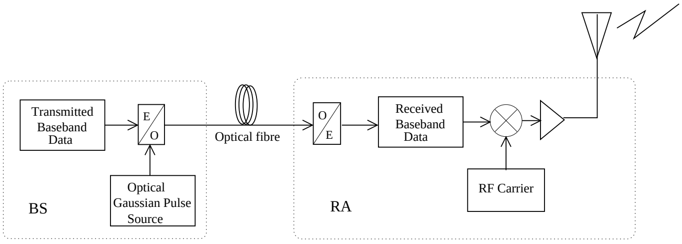

Fig. 2. System architecture of the DFO link, showing a single optical fibre link spanning from the BS to the RA. The transmitted baseband data is used to modulate a stream of optical Gaussian pulses, where an ideal optical modulator is assumed, therefore it does not impose any chirp on the optical pulse. Then the Gaussian optical signalling pulses are transmitted through the optical fibre, which imposes both linear and nonlinear distortions. At the RA, after an ideal photo-detector, the optical signalling pulses are converted back to the corresponding baseband electronic signals.

rather than simply assuming a perfect optical fibre. The phase rotation imposed by the optical fibre link on the modulated signal constellation diagram is supposed to be compensated, hence in this paper we only considered the fibre-induced imperfections imposed on the modulated signal's amplitude. Hence, the signal received at the RA i after passing through the realistically modelled optical fibre may be written as:

$$s_i = A_L x_i + n_f, \tag{1}$$

where A_L, x_i and $n_f \sim \mathcal{CN}(0, \sigma_f^2)$ represent the received amplitude of the optical pulse after passing through the optical fibre having a total length of L, the transmitted signal and the complex-valued Additive White Gaussian Noise (AWGN), respectively. Furthermore, the so-called *pulse-broadening* (PB) effect caused by dispersion [24] may not impose a significant performance limitation in pure optical fibre links, since the inter-pulse-interference may be negligible for the transmission of the baseband signal through the DFO link. However, the PB additionally imposes an attenuation of the optical signalling pulse, which may affect the attainable throughput of the cell-edge area, when considering our DFO link aided DAS combined with FFR in a multicell, multiuser scenario.

To elaborate on our optical fibre model a little further, the parameter A_L takes into account the fibre's attenuation, its dispersion and the fibre's nonlinearity characterized by the generalized Nonlinear Schrödinger (NLS) equation [22] expressed in the form of:

$$\begin{aligned}\frac{\partial A}{\partial z} =& \underbrace{\left(\frac{\beta_3}{6}\frac{\partial^3}{\partial t^3} - \frac{i\beta_2}{2}\frac{\partial^2}{\partial t^2} - \frac{\alpha}{2}\right)}_{\widehat{D}} A \\ &+ \underbrace{i\xi\left(|A|^2 + \frac{i}{\omega_0}\frac{1}{A}\frac{\partial}{\partial t}\left(|A|^2 A\right) - T_R\frac{\partial |A|^2}{\partial t}\right)}_{\widehat{N}} A, \end{aligned} \tag{2}$$

where $A(z,t)$ is the Gaussian signalling pulse envelope as a function of both the time t and the propagation distance z. The term $\widehat{D}$ characterizes the dispersion and fibre loss effects, while $\widehat{N}$ characterizes the nonlinearity effects, as the pulse propagates along the optical fibre. Still considering Eq (2), in the term $\widehat{D}$, α represents the fibre attenuation, β_2 is the group-velocity dispersion (GVD) parameter, and β_3 is the third-order dispersion coefficient, which becomes significant for ultra-narrow signalling pulses, as detailed in [24]. Considering the term $\widehat{N}$ in Eq (2), ξ describes the fibre's nonlinearity, ω_0 is the angular frequency of the carrier wave and T_R is related to the slope of the Raman gain spectrum, as detailed in [22]. In the case of having a pulse width of $T_0 > 5$ps which is typical for telecommunication fibres [22], the first term of $\widehat{D}$ and the last two terms of $\widehat{N}$ may be neglected [22]. These simplifications allow us to focus our attention on the nonlinearity and dispersion effects in this paper, hence the fibre loss parameter is assumed to be $\alpha = 0$. Then Eq (2) may be further simplified to:

$$\frac{\partial A}{\partial z} = \left(-i\frac{\beta_2}{2}\frac{\partial^2}{\partial t^2} + i\xi|A|^2\right) A = \left(\widehat{D'} + \widehat{N'}\right) A, \tag{3}$$

where the terms $\widehat{D'}$ and $\widehat{N'}$ are the simplified forms of the dispersion character $\widehat{D}$ and of the nonlinear character $\widehat{N}$ in Eq (2).

More explicity, the general formula of Eq (2) or its simplified form in Eq (3) describes the pulse propagation problem [22], but in this form it is not directly suitable for analyzing how the throughput of the wireless link is affected by the parameters of the imperfect optical fibre backhaul. The more practical SSF may be applied for analyzing the solutions of the NLS equation [22], which has been considered for modelling the optical-fibre communication systems [25]. Hence we employ the SSF method for jointly analyzing the attainable throughput of the DFO link. The SSF method delivers an approximate numerical solution, where the dispersive and nonlinear effects observed in Eq (3) may be separated into independent phenomena over a small segment-length l stretching from z to $(z+l)$ in Eq (3), yielding:

$$A(z+l,t) \approx F_T^{-1}\left\{exp\left[l\widehat{D'}(-i\omega)\right] F_T\left[exp(l\widehat{N'})A(z,t)\right]\right\}, \tag{4}$$

where F_T and F_T^{-1} denotes the Fourier-transform and inverse Fourier-transform operation, respectively. Firstly, the exponential nonlinearity-related term $exp(l\widehat{N'})$ of Eq (4) may be taken into account directly in the time domain. Secondly, before characterizing the dispersive effects, we take the Fourier-transform of the term $exp(l\widehat{N'})A(z,t)$, since the exponential dispersion-related term $exp(l\widehat{D'})$ may be evaluated in the frequency domain. The Fourier-transform of the dispersion character $\widehat{D'}$ is obtained by replacing the operator $\partial/\partial T$ by $-i\omega$ in Eq (3). Then, following the inverse Fourier-transform of Eq (4), we obtain the time domain representation of the received signal after propagating through the l-length fibre. The total optical fibre length satisfies $L = ml$, which suggests that the whole fibre length is decomposed into m consecutive l-length segments. Hence the optical pulse propagating through an L-length fibre may be obtained by evaluating Eq (4) in m consecutive steps, yielding a solution denoted as A_L.

III. Received Signal of DFO Aided DAS with FFR Systems

A. DFO aided Non-Cooperative DAS with FFR system

Focusing our attention on the cell B_0 of Fig. 1, when non-cooperative DASs are employed, the transmit power P_B of the BS and the transmit power P_R of each RA should obey the total transmit power constraint of $P_B + N_r P_R = P$, where P is the full power at the BS of the traditional UFR and FFR scheme.

1) Received Signal in the Cell-Centre Area: The interference at any MS located at point Z_i in the cell-centre area is imposed by the direct wireless links of BSs $\{1, \ldots, N_b\}$, with N_b being the number of BSs, which we refer to as the Inter-BS-Interference (IBI). Hence, the received signal may be written as:

$$y_c = \sqrt{P_B}\psi_{B0}h_{B0}x_0 + \sum_{j=1}^{N_b} \sqrt{P_B}\psi_{Bj}h_{Bj}x_j + n, \quad (5)$$

where ψ_{Bj}, h_{Bj}, $j \in [0, N_b]$ and $n \sim \mathcal{CN}(0, \sigma_0^2)$ represent the combined pathloss plus shadowing based large-scale signal attenuation, small-scale fast Rayleigh fading and the complex-valued AWGN, respectively. More explicitly, we jointly consider both the pathloss and the lognormal shadowing component, which is formulated as: $\psi_{Bj} = [\rho 10^{\varsigma(\sigma_s)/10}]^{1/2}, j \in [0, N_b]$, where ρ denotes the pathloss that obeys a predefined pathloss model [26], while ς denotes a real valued Gaussian random variable having a standard deviation of $\sigma_s = 8$ dB [26]. Hence, $G_{Bj} = \psi_{Bj}|h_{Bj}|$ denotes the equivalent channel gain, while the SINR of any of the MSs near the cell-centre is given by:

$$\gamma_c = \frac{G_{B0}^2 P_B}{2\sigma_0^2 + \sum_{j=1}^{N_b} G_{Bj}^2 P_B}. \quad (6)$$

2) Received Signal in the Cell-Edge Area: When considering the cell-edge area, we assume that the links spanning from the BS B_0 of Fig. 1 to the RAs are constituted by a realistic imperfect optical fibre, while the last-mile connection from the RAs to the MS relies on the wireless link. The signal received at the RA i after passing through the realistically modelled optical fibre is introduced in Section II-B.

The noise-contaminated, faded signal $s_i, i \in [1, N_r]$ denoted in Eq (1) at the wireless channel's input is normalised by a power-scaling factor and then forwarded through the wireless channel to the destination, namely to the MS roaming in the cell-edge area, where the power-scaling factor χ is employed in order to maintain a constant transmit power at the RAs. As a result, the signal received by MS i at any point Z_i in the cell-edge area in the absence of any cooperative techniques, may be written as

$$y_{ei} = \sqrt{P_R}\psi_{Ri}h_{Ri}\chi s_i + \sum_{k=1,k\neq i}^{N_r} \sqrt{P_R}\psi_{Rk}h_{Rk}\chi s_k + n. (7)$$

Let $A = \chi A_L$ and $N_f = 2\sigma_f^2\chi^2$ denote the equivalent optical fibre-induced amplitude attenuation and the equivalent power spectral density of the optical fibre noise, respectively. The details of the parameters s_i and A_L are introduced in Section II-B. Then, the SINR at any MS roaming in the cell-edge area is:

$$\gamma_{ei} = \frac{G_{Ri}^2 A^2 P_R}{2\sigma_0^2 + \sum_{i=1}^{N_r} G_{Ri}^2 N_f P_R + \sum_{k=1,k\neq i}^{N_r} G_{Rk}^2 A^2 P_R}, (8)$$

where $G_{Ri} = \psi_{Ri}|h_{Ri}|$ denotes the equivalent channel gain.

3) Idealistic Received Signal in the Cell-Edge Area: We assume the employment of perfect adaptive beamforming, where each MS is served with the aid of a narrow beam. We also assume that the MSs would be served only by the nearest RAs and that their reception is not contaminated by the other RAs, hence no IRI is received by the MSs roaming in the cell-edge area. Hence their reception is only contaminated by the noise N_f imposed at the optical fibre receiver. Then the interference-free upper bound of the SINR can be rewritten from Eq (8) as:

$$\gamma_u = \frac{G_{Ri}^2 A^2 P_R}{2\sigma_0^2 + G_{Ri}^2 N_f P_R}. \quad (9)$$

4) Benchmarker Systems: Finally, when the classic UFR technique is employed, the received signal model is described by Eq (5), but bearing in mind that the full power P is transmitted by each BS instead of P_B. When the FFR technique is employed, similarly to the classic UFR, the signal received in the cell-centre area is also described by Eq (5). On the other hand, the signal received in the cell-edge area both from the serving BS and from the cells using the same frequency band in tier-two obeys Eq (5).

B. DFO aided Cooperative DAS with FFR

In a multicell, multiuser scenario cooperative DAS techniques may be used, in order to provide a high throughput for the MSs roaming near the cell-edge area, especially for mitigating the worst-case direction problem caused by IRI. To simplify the entire system, only a single omni-directional antenna is applied for each RA. Nonetheless, when jointly designing the TPP matrix $\mathbf{T}$, the N_R cooperative RAs operate in a concerted action as a virtual multiple-input and single-output (MISO) or virtual multiple-input and multi-output (MIMO) system. On the other hand, only a single receiver antenna is applied at the MS. We will show that the proposed system architecture is capable of substantially enhancing the throughput achievable in the cell-edge area with the advent of our cooperative TPP aided FFR scheme.

Notation: the lower case boldface letters and the upper case boldface letters represent column vectors and matrices, respectively. The superscript $(\cdot)^T$ and the $(\cdot)^H$ denotes the transposition and the conjugate transpose respectively.

1) Received Signal-to-Interference-plus-Noise-Ratio: The principle of cooperative DAS schemes is essentially the same as that of cooperative BSs [8], where the transmit signal destined for the MSs is spread over all the N_r cooperative RAs. In the multicell multiuser scenario there are N_m MSs roaming in the cell-edge area of Fig 1, which are simultaneously supported by the N_r RAs ($N_r = N_m$). Provided that the different propagation delays of all the N_r RA links measured with respect to all the served N_m MSs can be pre-compensated, the vector of received signal can be written as:

$$\mathbf{y} = \mathbf{HTx} + \mathbf{n}, \tag{10}$$

where $\mathbf{y}_{N_m \times 1}$ and $\mathbf{n}_{N_m \times 1}$ denote the received signal vector and the circularly symmetric complex Gaussian noise vector. Furthermore, $\mathbf{x} = [x_1, x_2, \cdots, x_{N_m}]^T_{1\times N_m}$, x_i is defined as the signal transmitted from RA i to MS i. More explicitly, $x_i = \chi_i s_i$, $i \in [1, N_r]$ represents the signal passing through the realistic 'lossy' optical fibre, where χ_i and s_i is the same as that defined in Section III-A.2. If the central BS has an estimate of the channel matrix $\mathbf{H} = [\mathbf{h}_1^T, \mathbf{h}_2^T, \cdots, \mathbf{h}_{N_m}^T]^T_{N_m \times N_r}$, we can design a transmit matrix $\mathbf{T}$ for mitigating the IRI, where $\mathbf{T} = [\mathbf{t}_1, \mathbf{t}_2, \cdots, \mathbf{t}_{N_m}]_{N_r \times N_m}$ is uniquely and unambiguously determined by $\mathbf{H}$. We also have a dedicated TPP matrix $\mathbf{T}$, which obeys the per RA power constraint of:

$$\mathbf{T}_{i,\forall}\mathbf{T}_{i,\forall}^H \leq \frac{P - P_B}{N_r}, \tag{11}$$

where $\mathbf{T}_{i,\forall}$ is the row vector of the matrix $\mathbf{T}$.

Furthermore, $\mathbf{h}_i = [\psi_1 h_1, \psi_2 h_2, \cdots, \psi_{N_r} h_{N_r}]_{1\times N_r}, i \in [1, N_m]$, represents the channel of all the N_m RA to MS i links, which takes into account both the large-scale signal attenuation and the small-scale fast Rayleigh fading channel, where ψ_i and h_i is the same as that defined in Section III-A.2. Hence, a unified discrete-time model for the signal received by MS i may be formulated based on Eq (10) as:

$$y_i = \|\mathbf{h}_i \mathbf{t}_i\| x_i + \sum_{k \neq i} \|\mathbf{h}_i \mathbf{t}_k\| x_k + n_i. \tag{12}$$

When we have $k \neq i$, x_k is the IRI imposed by the transmit signal intended for MS k, but received at MS i. Hence, the DFO links' SINR encountered at MS i in the cell-edge area may be written as:

$$\gamma_i = A^2 \mathbf{h}_i \mathbf{t}_i \mathbf{t}_i^H \mathbf{h}_i^H \times \\ [2\sigma_0^2 + \underbrace{N_f \mathbf{h}_i \mathbf{t}_i \mathbf{t}_i^H \mathbf{h}_i^H}_{IRI_2} + \underbrace{(A^2 + N_f)\mathbf{h}_i (\sum_{k\neq i} \mathbf{t}_k \mathbf{t}_k^H)\mathbf{h}_i^H}_{IRI_1}]^{-1}, \tag{13}$$

where A and N_f represent the equivalent optical fibre attenuation factor and the equivalent power spectral density of the optical fibre' noise, respectively, as defined in Section III-A.2. It can be seen from Eq (13), that for MS i, the IRI is composed of two terms. Specifically, the term IRI_1 of Eq (13) is the desired signal of MS $k \neq i$ that is also contaminated by the optical fibre link's noise N_f, which can be mitigated by appropriately designing the corresponding TPP matrix. The other term, namely IRI_2 of Eq (13), is the optical fibre link's noise contaminating the desired signal of MS i, which is the self-inflicted noise, hence the TPP matrix is unable to mitigate it.

2) Linear Transmit Processing: Again, we assume that there is only a single transmit antenna at each RA and a single receive antenna at each MS, hence our system is fully described by the number of RAs N_r and by the number of MSs N_m served. Hence our design is based on the $(N_m \times N_r)$-element channel matrix $\mathbf{H}$ associated with the central BS and the TPP facilitates a low-complexity matched-filter-based receiver design at each MS. Our linear TPP matrix $\mathbf{T}$ may be written as:

$$\mathbf{T} = \mathbf{G} \cdot \mathbf{W}, \tag{14}$$

where $\mathbf{W}_{N_m \times N_m}$ is a diagonal matrix representing the power [8] allocated for each RA and $\mathbf{G}_{N_r \times N_m}$ is the linear TPP matrix jointly designed on the basis of $\mathbf{H}$. The TPP matrix $\mathbf{G}$ can be calculated with the aid of different linear preprocessing algorithms. In this paper we consider the minimum mean square error (MMSE) beamformer [27] and the eigenbeamformer (egBF) [28] as our design example.

The classic MMSE beamforming technique strikes an attractive tradeoff between the achievable interference cancellation and noise enhancement, hence it is attractive for practical applications. The TPP weight matrix $\mathbf{G}_{MMSE} = \mathbf{H}^H(\mathbf{HH}^H + \frac{2\sigma_0^2}{P_R}\mathbf{I})^{-1}$, which is entirely based on the channel matrix $\mathbf{H}$, remains unaffected by the transmit signal. The employment of the TPP matrix $\mathbf{G}_{MMSE}$ mitigates the IRI_1 component in Eq (13), eliminating the interference inflicted on the desired signal.

In cooperative egBF, the TPP matrix $\mathbf{G}_{BF} = [\mathbf{g}_1, \mathbf{g}_2, \cdots, \mathbf{g}_{N_m}]$ is used, where $\mathbf{g}_i, i \in [1, N_m]$ is the right-hand-side singular vector of $\mathbf{H}$, which only achieves a power gain, while the mitigation of the term IRI_1 in Eq (13) is dependent on the instantaneous geographic distribution of the users. Hence the mitigation of the IRI_1 cannot always be achieved by appropriately selecting the direction of the transmitted beam, unless we employ an idealistic infinitesimally narrow beam for each MS. The associated performance will be characterized in Section IV-E.

However, in contrast to the IRI_1, the link's self-noise imposed by the optical fibre receiver's noise contribution, namely the IRI_2 terms of Eq (13) cannot be mitigated by the TPP matrix employed, regardless, whether the cooperative MMSE or the cooperative egBF is used. In fact, the self-interference may even be boosted, when the desired signal of MS i is amplified.

C. System Throughput

Let us now demonstrate how these SINR expressions may be mapped to the ultimate system performance metric formulated in terms of the achievable throughput η. The throughput may be characterised by the maximum *successfully transmitted* information rate, which is referred to as the system's *goodput*:

$$\eta(\gamma) = R_M R_C [1 - P_{bl}(b, \gamma)], \tag{15}$$

where γ may represent either γ_c of Eq (6) or γ_{ei} of Eq (8) or γ_u of Eq (9), R_M denotes the 'rate' i.e. the throughput of the modulation scheme, while R_C is that of the channel code. Still referring to Eq (15), $P_{bl}(b, \gamma)$ represents the BLock Error Ratio (BLER) corresponding to the particular Modulation and Coding Scheme (MCS) employed. In this paper, we assume that Bit Interleaved Coded Modulation (BICM) [29] is employed, which relies on Gray mapped M-ary Quadrature Amplitude Modulation (QAM) [30], where we have $M = 2^b$ and $b = 2, 4, 6$ represents the number of bits per QAM symbol. Hence the modem's throughput is $R_M = b$. In our paper, we employ 2^b-ary QAM combined with Rate Compatible Punctured Codes (RCPC) [31] having six selected MCSs, namely Mode $[1, \ldots, 6]$ of $[R_M, R_C] = [(2, 1/2), (2, 3/4), (4, 1/2), (4, 3/4), (6, 2/3), (6, 6/7)]$.

In practice, obtaining the BLER curves for all the MCSs by simulation is time-consuming, especially in our multicell multiuser system-level evaluations. Let us hence circumvent this time-consuming process with the aid of a more efficient semi-analytical process. We commence by briefly highlighting the derivation of the BLER $P_{bl}(b, \gamma)$ of a 2^b-ary QAM aided BICM scheme based on the BLER $P_{bl}(b = 1, \gamma_0)$ of a BPSK modulated BICM scheme transmitting over an AWGN channel, where only $P_{bl}(b = 1, \gamma_0)$ is evaluated by simulation. To this effect, we first define the appropriate *base-line* SINR γ_0 as that of a binary BPSK scheme, at which we have the same BLER as an arbitrary b-bit/symbol modem, which would typically require an SINR of $\gamma > \gamma_0$, i.e. where we have $P_{bl}(b, \gamma) = P_{bl}(b = 1, \gamma_0)$. We note that the above-mentioned BLER equality holds only, when the mutual information per bit output by the demodulator obeys the relation of $I(b, \gamma) = I(b = 1, \gamma_0)$. This is because I serves as the input of the channel decoder, and as long as I remains the same, the ultimate BLER also remains the same. Hence, the mutual information I per bit may be expressed as [29]:

$$I(b,\gamma) = 1 - \frac{2^{-b}}{b}\sum_{i=1}^{b}\mathbb{E}_w \times \left\{ \ln\left[1 + \sum_{j=1, j\neq i}^{b} \exp\left(-\frac{|u_j - u_i + w|^2 - |w|^2}{1/\gamma}\right)\right]\right\}, \tag{16}$$

where $w \sim \mathcal{CN}(0, 1/2\gamma)$ is the complex-valued zero-mean Gaussian noise process and $u \in \mathcal{A}$ represents the constellation points in the QAM alphabet, with the ith bit $\mathcal{A}$ being represented by $u_i, i \in [1, b]$. When fixing the mutual information per bit as $I(b, \gamma) = I(b = 1, \gamma_0)$, we may find the *base-line* SINR γ_0 for $b = 1$, where this BPSK modulated scheme achieves the same per-bit mutual information (MI) I as a higher-throughput 2^b-ary QAM-aided BICM scheme. More explicitly, the MI per pit $I(b = 1, \gamma_0)$ is a monotonically increasing function of γ_0, its unique inverse exists. Hence this *base-line* SINR γ_0 may be expressed as the inverse-function $\gamma_0 = I^{-1}[b = 1, I(b, \gamma)]$. This reveals the relation between γ and γ_0, allowing us to find the BLER $P_{bl}(b, \gamma)$ of a 2^b-ary QAM-aided BICM scheme from that of the simulated BLER of a BPSK modulated BICM scheme, i.e. from $P_{bl}(b = 1, \gamma_0)$, which may be formulated as:

$$P_{bl}(b,\gamma) = P_{bl}\left\{b = 1, I^{-1}[b = 1, I(b, \gamma)]\right\}. \tag{17}$$

As a result, the BLER $P_{bl}(b, \gamma)$ of the above MCSs may be obtained with the aid of Eq (17), where $P_{bl}(b = 1, \gamma_0)$ is obtained from the Monte-Carlo simulation of a BPSK modulated BICM scheme employing the above-mentioned RCPC having constituent code-rates of $R_C = [1/2, 3/4, 2/3, 6/7]$ in an AWGN channel. Finally, the associated effective throughput $\eta(\gamma)$ of Eq (15) expressed in terms of 'bits/s/Hz' may be obtained by assuming a Nyquist roll-off factor of zero. Owing to space limitations, the detailed link-level simulation results are not explicitly shown here.

TABLE I
PROPAGATION REGIMES

Curve	P_0	T_0	l	L_D	L_N
1	10mW	10ps	5m	5km	50km
2	160mW	10ps	5m	5km	3km
3	10mW	10ps	10m	5km	50km
4	10mW	20ps	5m	20km	50km
5	10mW	50ps	5m	125km	50km

IV. Performance Evaluation

A. Simulation Assumptions

The system topology considered is illustrated in Fig. 1, where each hexagonal cell has a radius of R, and the distance between the two adjacent BSs is $D = \sqrt{3}R$, e.g. $\overline{B_2B_3} = \sqrt{3}R$. We considered the Urban-Macro propagation scenario of [26], where we have $D = 3km$ and the distance-dependent pathloss expressed in dB is $34.5 + 35\log_{10}(d_0)$, with d_0 being the distance between any transmitter and receiver in meters. We assume furthermore that the total transmitter power is $P = 46$dBm and the noise power at the MS is -174dBm/Hz, when an operating in bandwidth of 10 MHz is considered [26]. Moreover, the optical fibre link's normalised Signal-to-Noise-Ratio (SNR) is assumed to be 50dB and the length of the optical fibre is assumed to be five times the distance between the BS and RA, where we have $L = 5d$, and d is the line-of-sight distance. We opted for $d = 0.7R, \forall i$.

The cell-centre area's radius r may be defined as the maximum radius, where a throughput of at least $\eta = 2bits/s/Hz$ may be maintained in a conventional cellular system employing the classic UFR technique, but beyond this coverage-radius it drops below $\eta = 2bits/s/Hz$. When employing DASs in a FFR-based cellular system, the transmit power of the BS should be sufficiently high to ensure that the average throughput maintained at a distance of r remains exactly as high as that of the classic UFR technique, while the rest of the power is evenly allocated to the RAs. Hence, when considering the $N_r = 6$ RAs operating in a non-cooperative DAS aided FFR scenario, the resultant power sharing regime of all the transmitters obeys $P_B = 2P/5$, while for the relay we have $P_R = P/10$. By contrast, when considering the $N_r = 6$ RAs operating in a cooperative DAS assisted FFR scenario, the power constraint of Eq (11) is applied. Finally, the ultimate throughput is obtained by averaging the SINR over 4000 simulation runs, and then substituting it into Eq (15) and Eq (17).

B. Propagation Regimes in the DFO Link

Before detailing our results, the propagation scenario encountered has to be introduced. When the pulses propagate

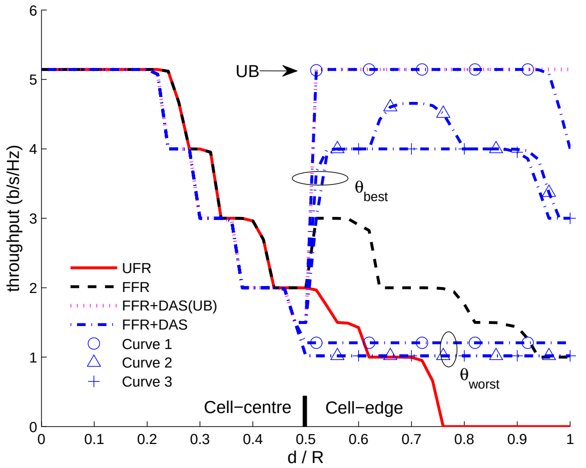

Fig. 3. Throughput comparison of the traditional UFR system, FFR system and of the $N_r = 6$ non-cooperative DAS aided FFR system in two-tier scenarios along the θ_{best} and θ_{worst} directions recorded for characterizing the nonlinear effects of the optical fibre and the accuracy of the SSF Method.

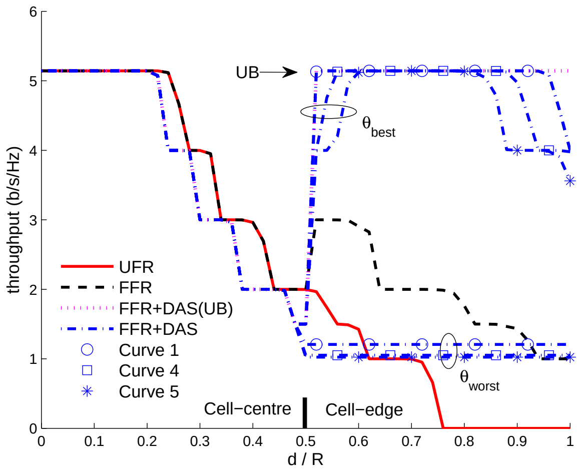

Fig. 4. Throughput comparison of the traditional UFR system, FFR system and of the $N_r = 6$ non-cooperative DAS aided FFR system along the θ_{best} and θ_{worst} directions for characterizing the dispersion effects of the optical fibre.

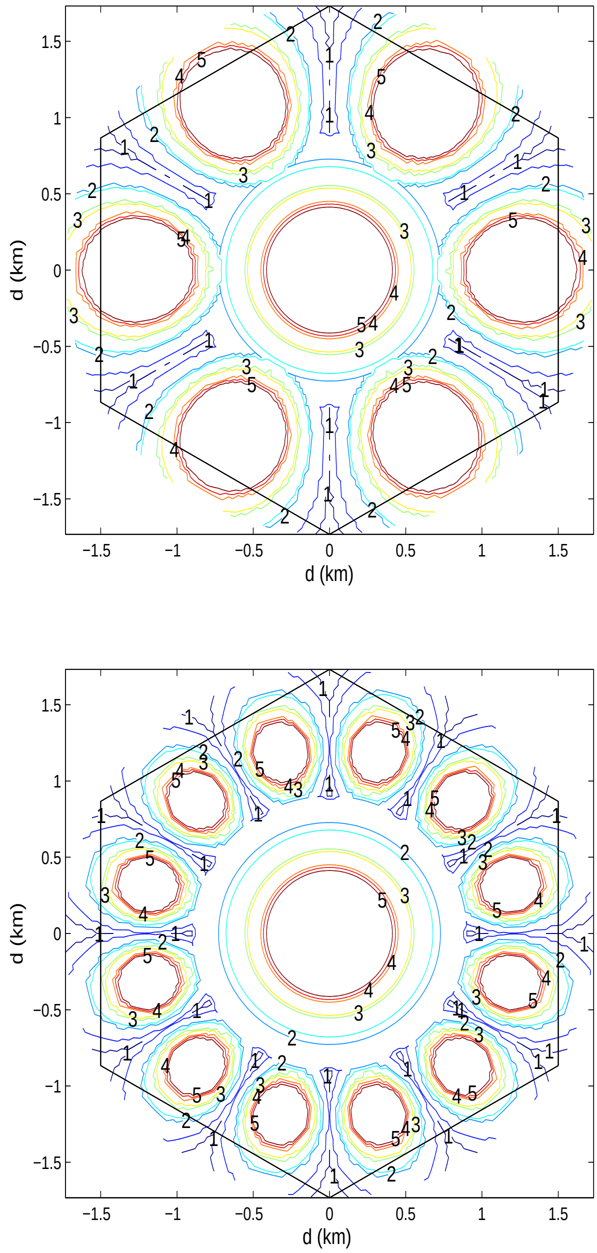

Fig. 5. Throughput contours for the $N_r = 6$ and $N_r = 12$ non-cooperative DAS aided FFR system.

along the optical fibre, both the nonlinearity and the dispersion depend on the peak power P_0 and on the initial width T_0 of the incident pulse. The critical fibre-lengths L_N and L_D quantify the length of fibre over which either the nonlinear, or the dispersive effects become dominant during the signalling pulse's propagation. The relations between L_N and P_0, L_D and T_0 are calculated as follows [22]:

$$L_N = \frac{1}{\xi P_0}, L_D = \frac{T_0^2}{|\beta_2|}. \tag{18}$$

The typical values of the GVD parameter β_2 and the nonlinearity parameter ξ at a wavelength of $1.55\mu m$ are [22] $|\beta_2| \approx 20ps^2/km$ and $\xi \approx 2W^{-1}km^{-1}$ for standard telecommunication fibres. For a given optical fibre length of L, we have:

- if $L \ll L_N$ and $L \ll L_D$, neither the nonlinear nor the dispersive effects impose a significant performance degradation during the pulse's propagation.
- if $L \ll L_N$ and $L \sim L_D$, the nonlinear effects may be ignored and the the dispersion will play the dominant role.
- for $L \sim L_N$ and $L \ll L_D$, the dispersion is negligible compared to the nonlinear distortion.
- for $L \sim L_N$ and $L \sim L_D$, both of the nonlinear and dispersion effects are non-negligible.

In this paper, according to the Urban-Macro cell scenario introduced in Section IV-A, we assume the set of P_0 and

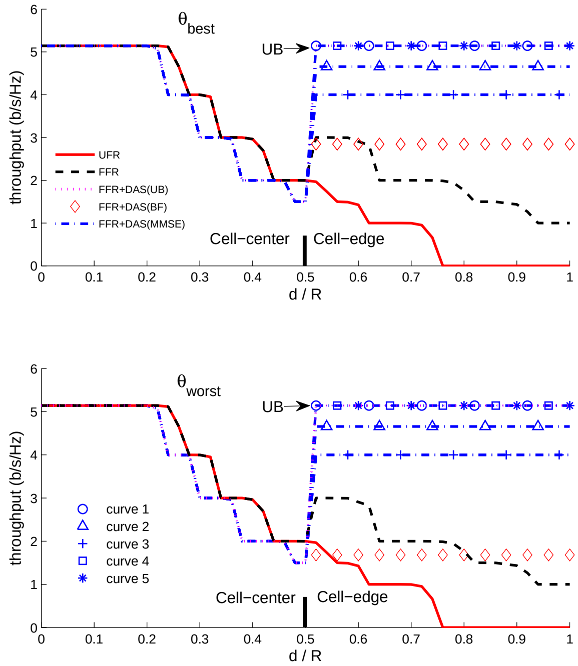

Fig. 6. Throughput comparison of the traditional UFR system, FFR system and the $N_r = 6$ cooperative DAS aided FFR system along the best direction with 5 sets of optical parameters in Table I multicell multiuser scenario. The legends are shared between the top and bottom graphs.

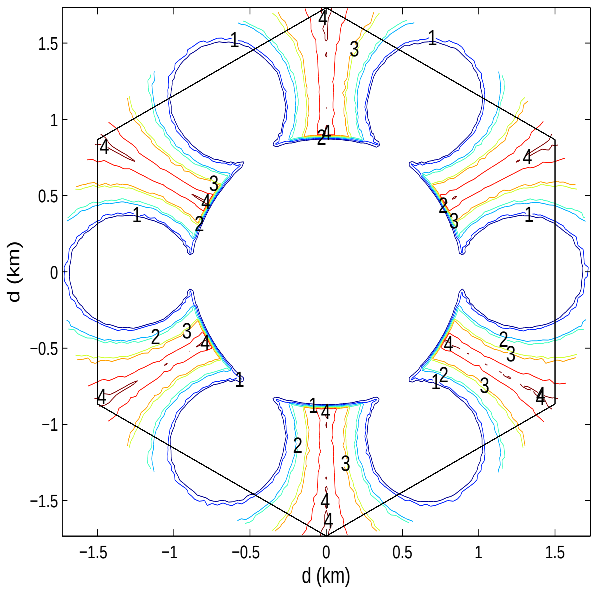

Fig. 7. The enhancement of throughput $\Delta\eta$ contours for the $N_r = 6$ cooperative DAS aided FFR systems, comparing with non-cooperative DAS aided FFR.

T_0 values shown in Table I in order to investigate how the nonlinear and dispersion effects of the optical fibre influence the attainable throughput of the wireless channel in the cell-edge area.

C. *Throughput of Cell-centre Area*

The attainable throughput of both of the non-cooperative DAS combined with FFR system (Fig. 3 and 4) and the cooperative DAS combined with FFR (Fig. 6 in the cell-centre area rely on the same SINR of Eq (6) introduced in Section III-A. Hence, both of them have the same throughput performance. Explicitly, upon assigning a transmit power of $P_B = 2P/5$ in the cell-centre area, the throughput of the non-cooperative DAS combined with FFR system and that of cooperative DAS combined with FFR become similar to that of the traditional UFR and FFR systems, provided that the latter two systems assign the full transmit power to the BS.

D. *Cell-edge Area of Non-cooperative DAS with FFR*

Fig. 3 and Fig. 4 compare the throughput of the classic UFR system, of the traditional FFR system and of the non-cooperative RA-aided FFR assisted systems using $N_r = 6$, $N_m = 6$ in the best and the worst direction in a two-tier scenario. The four sets of optical fibre parameters shown in Table I were used.

1) Throughput along Best Direction: By contrast, when the cell-edge area is considered, observe in Fig. 3 and Fig. 4 that the throughput of the conventional UFR scheme becomes lower than $\eta = 2$ bits/s/Hz, while that of the conventional FFR scheme is in the range of $\eta \in [1, 3]$ bits/s/Hz. When the non-cooperative RA-aided FFR-assisted system is employed in conjunction with $N_r = 6$ RAs, a throughput in the range of $\eta \in [3, 5]$ bits/s/Hz is achieved along the best direction.

More explicity, when using the parameters of Table I, Curves 1 - 5 in Fig. 3 and Fig. 4, suggest that:

- *Nonlinear Effect of the DFO Link*: The comparison of Curve 1 ($P_0 = 10$mW) and Curve 2 ($P_0 = 160$mW) in Fig. 3 shows how the power assigned to the optical pulses affects the throughput of the wireless link, which was demonstrated by setting $P_0 = 10$mW and 160mW of peak power for the optical signalling pulse. Again, the corresponding optical parameters are shown in Table I. Observe by comparing Curves 1 and 2 of Fig. 3 that assigning a $P_0 = 160$mW power to the optical pulse makes the nonlinearity-induced impairments dominant, which will broaden the spectrum of the optical pulse in the frequency domain. The nonlinearity indirectly results in an increased attenuation for the optical pulses, but this cannot be compensated by an increased transmit power, hence this leads to a boost of the IRI. As a net-result, the system suffers from an approximate throughput loss of 1 bits/s/Hz in the cell-edge area along the best direction.
- *Accuracy of SSF Method*: Comparing Curve 3 to Curve 1 of Fig. 3, the former is associated with a longer segment l used by the SSF method, which reduces the analysis complexity. However, as a result, the predicted throughput is reduced by about 1 bits/s/Hz. By contrast, a shorter

segment l results in a more accurate of the SSF model at the cost of a higher offline analysis complexity. But selecting the probable segment length will strongly affect the results of simulation, which is important for whom doing the relative research. For a typical urban cell size our Monte-Carlo simulation results suggest that $l = 5$m is an appropriate compromise, which may be trusted as the real attainable throughput of our DFO aided DAS combined with FFR system.

- *Dispersion Effect of the DFO Link*: Fig. 4 demonstrates by increasing the width of the optical signalling pulse from $T_0 = 10$ps to 20ps and 50ps for Curves 4 and 5, how this affects the throughput of the wireless link, when the non-cooperative RA-aided FFR-assisted system is employed in conjunction with $N_r = 6$ RAs. Again, when using the optical parameters shown in Table I and setting a peak power of $P_0 = 10$mW, the nonlinear effects of the optical fibre become negligible. Comparing Curve 4 ($T_0 = 20$ps) and 5 ($T_0 = 50$ps) to Curve 1 ($T_0 = 10$ps) of Fig. 4, the throughput at the cell-edge remains in the range of $\eta \in [4, 5]$ bits/s/Hz, but when the optical pulse width is increased, according to Table I from $T_0 = 10$ps to 20ps and 50ps, the attainable throughput of the cell-edge area is reduced. The reason for this observation is that wide pulses are typically broadened to a lesser relative degree along the optical fibre, which also leads to a reduced attenuation both at the optical receiver of the serving RA as well as at the interfering RAs.

2) Throughput along Worst Direction: When considering the worst direction in both Fig. 3 and Fig. 4, regardless of the specific choice of the five parameter sets of Table I, we only achieve a throughput of about $\eta = 1$ bits/s/Hz. This is due to the above-mentioned worst-case direction problem [6], which becomes the limiting factor in the case of the conventional non-cooperative RA-aided FFR assisted system.

3) Comparison of the Entire Cell's Throughput: Fig. 5 demonstrates the attainable throughput across the entire cell for the different configurations of our non-cooperative RA-aided FFR assisted system associated with Curve 1 of Table I. More explicity, the cell-centre area's throughput contours recorded in Fig. 5 for both configurations are similar. However, the throughput distribution of the $N_r = 6$ RA-aided configuration recorded for the cell-edge area tends to be more 'patchy', while that of the $N_r = 12$ RA-assisted configuration tends to cover the entire outer ring more evenly. As a result, the general conclusion emerging for the comparison of these two configurations is that the optimum positioning of DASs should take into account the expected user-distribution and user-load. However, the "worst-case direction" problem persists in both of these two configurations.

E. Cell-edge Area of Cooperative DAS with FFR

Fig. 6 compares the throughput of the classic UFR based arrangement and of the traditional FFR aided system, as well as of the cooperative RA-aided FFR assisted system using $N_r = 6$, which was evaluated along both the best and worst angular directions respectively and employing the five sets of parameters seen in Table I for the optical fibre link. We consider supporting $N_m = 6$ MSs roaming in the cell-edge area, where MS i is close to the RA i. The N_m MSs are served simultaneously by the N_r cooperative RAs and they are randomly distributed around the point $Z_i, i = 1, \ldots, N_m$ of Fig. 1, where Z_i belongs to the corresponding $60°$-sector surrounding RA i. The MSs are allowed to randomly cross the cell-edge area, but only once, in order to investigate the histogram of the attainable throughput for the N_m MSs.

1) Throughput along Best Direction: When the cell-edge area is considered, observe the upper figure in Fig. 6 that the throughput of the conventional UFR scheme becomes lower than $\eta = 2$ bits/s/Hz, while that of the conventional FFR scheme is in the range of $\eta \in [1, 3]$ bits/s/Hz. When the co-operative RA-aided FFR-assisted system using the parameters associated with Curves 1, 4 and 5 of Table I is considered, observe in Fig. 6 that linear TPP achieves a throughput of $\eta = 5$ bits/s/Hz, which is similar to the throughput upper bound of the RA-aided FFR-assisted system. Hence, when the nonlinearity effects can be ignored, the dispersion does not overly affect the throughput of the wireless channel.

Comparing Curve 2 and Curve 1 in Fig. 6, when using a peak power of $P_0 = 160$mW for the signalling pulses, the MMSE TPP techniques achieve a slightly higher throughput than 4 bits/s/Hz. Since the term IRI_1 in Eq (13) is mitigated by the MMSE TPP, the throughput reduction is imposed by the further attenuation of the received optical signalling pulses inflicted by the fibre's nonlinearity. When employing the parameters associated with Curve 3 with a segment length of $l = 10$m for the SSF method, a throughput reduction of $\Delta\eta = 1$ bits/s/Hz is encountered.

Observe in Fig. 6 that the throughput of cooperative egBF is between that of the linear TPP techniques and of the traditional UFR system, and it is not always higher than that of the conventional FFR scheme. The reason for this phenomenon is that the performance of the cooperative egBF is also dependent on the geographic distribution of the N_m users. Hence the served MS may suffer from an increased interference, which imposes an increased throughput erosion in comparison to the conventional FFR scheme.

2) Throughput along Worst direction: It is demonstrated in the lower figure of Fig. 6 that the cooperative RA-aided FFR assisted system does not suffer from the worst-case angular direction problem and hence the linear TPP techniques achieve a throughput of $\eta = 5$ bits/s/Hz, which is the upper bound of the RA-aided FFR-assisted system. The other curves exhibit the same throughput performance as that shown in the upper figure of Fig. 6. The cooperative egBF does not solve the worst-case angular direction problem, hence its throughput is lower than that of the traditional FFR.

F. Enhancement of Throughput Across the Entire Cell

In order to observe the attainable throughput improvement $\Delta\eta$ achieved by the cooperative RA aided FFR assisted systems over their non-cooperative counterparts across the entire cell, the resultant throughput contour profile associated with Curve 1 of Table I is portrayed in Fig. 7. We configured the cooperative techniques for enhancing the attainable throughput in the cell-edge area, hence in the cell-centre area we have $\Delta\eta = 0$. In the cell-edge area, when considering the cooperative MMSE arrangement for example, there is a significant throughput improvement in the worst-case angular direction, since we have $\Delta\eta = 4$bits/s/Hz in the direction θ_{worst}. By contrast, when the MS is roaming close to the RA, the throughput improvement achieved by the cooperative MMSE technique remains limited. When however the MS is roaming far from the RA, the benefits of the cooperative techniques become more pronounced.

V. Conclusions

The achievable throughput of a DFO aided DAS relying on FFR and a realistic optical fibre backhaul was investigated in practical multicell, multiuser scenarios. Our work demonstrated that the non-cooperative DAS aided FFR system is capable of gleaning some benefits from the imperfections of the optical fibre, because the dispersion of the optical signalling pulse might indirectly increase the attainable throughput of the cell-edge area. More explicity, when applying the configurations of $N_r = 6$ and $N_r = 12$, the geographic throughput distribution becomes different, which may be beneficially exploited for supporting different geographic users-distributions. Correspondingly, the cooperative RA-aided FFR relying on the linear TPP techniques [1] advocated is capable of efficiently mitigating the IRI in the worst-case direction. As a result, the system may be capable of supporting a throughput of $\eta = 5$ bits/s/Hz, regardless of the specific geographic user-distribution encountered. Furthermore, the cooperative RA-aided FFR system may become tolerant to the dipsersion of the optical pulse, but sensitive to the fibre-induced nonlinearity, if the optical pulse has a high power.

References

[1] Y. Xiang, J. Luo, and C. Hartmann, "Inter-cell interference mitigation through flexible resource reuse in OFDMA based communication networks," *Proc. of European Wireless*, vol. 43, pp. 1–7, Apr. 2007.

[2] R. Zhang and L. Hanzo, "Wireless cellular networks," *IEEE Vehicular Technology Magazine*, vol. 5, pp. 31–39, 2010.

[3] H. Ekstrom, A. Furuskar, J. Karlsson, and et al, "Technical solutions for the 3G long-term evolution," *IEEE Communications Magazine*, vol. 44, pp. 38– 45, Mar. 2006.

[1]Indeed, efficient TPP requires efficient feedback control, which involves an accurate and frequent channel estimation, quantisation and feedback process, where sophisticated signal processing improvements may result in an increased throughput. The overhead associated with this cooperative transmission, or closed-loop design in general, is constituted by the Doppler-dependent channel-sounding pilot overhead and the feedback quantisation overhead, where the latter potentially depends not only on the quantisation method performed, but also on the specific cooperative structure employed, i.e. on whether centralised or distributed cooperation is used.

Regarding the effect of the numbers of RAs, an intuitive observation is that the more cooperative RAs, the more overhead will be incurred. However, no simple quantitative relationship may be established. Furthermore, since the amount of overhead imposed may offset the potential gain achieved, we have to strike an attractive tradeoff, as discussed in [32]. The rate of change of the channel will indeed significantly decrease the resultant performance gains, since the feedback may become more outdated and the preprocessing matrix will be subject to strong mismatch. Hence, closed-loop designs in general may not be suitable for high-velocity applications, where in addition to an increased normalized feedback delay, the channel estimation becomes more challenging in the downlink.

[4] A. Ghosh, D. Wolter, J. Andrews, and R. Chen, "Broadband wireless access with WiMax/802.16: current performance benchmarks and future potential," *IEEE Communications Magazine*, vol. 43, pp. 129–136, Feb. 2005.

[5] C. Wan and J. Andrews, "Downlink performance and capacity of distributed antenna systems in a multicell environment," *IEEE Transactions on Wireless Communications*, vol. 6, pp. 69– 73, Jan. 2007.

[6] X. Xu, R. Zhang, and L. Hanzo, "Imperfect radio-over-fibre aided cooperative distributed antennas with fractional frequency reuse," in *Proc. of IEEE Vehicular Technology Conference (VTC)*, Ottawa, Canada, September 2010, pp. 1–5.

[7] ——, "Digital RoF aided cooperative distributed antennas with FFR in multicell multiuser networks," in *Proc. of IEEE Vehicular Technology Conference (VTC)*, San Francisco, United States, Fall 2011, pp. 1–5.

[8] H. Zhang and H. Dai, "Cochannel interference mitigation and cooperative processing in downlink multicell multiuser MIMO networks," *EURASIP Journal on Wireless Communications and Networking*, vol. 2004, pp. 1687–1472, 2004.

[9] 3GPP TSG-RAN, "Futher advancements for E-UTRA; physical layer aspects," GPP Std. TR 36.814 v.0.4.1, Tech. Rep., 2009.

[10] M. Crisp, S. Li, A. Watts, R. Penty, and I. White, "Uplink and downlink coverage improvements of 802.11g signals using a distributed antenna network," *Journal of Lightwave Technology*, vol. 25, pp. 3388 – 3395, 2007.

[11] D. Wake, "Trends and prospects for radio over fibre picocells," in *Proc.of Microwave Photonics (MWP)*, 2002.

[12] D. Wake, M. Webster, G. Wimpenny, and et al, "Radio over fiber for mobile communications," in *IEEE International Topical Meeting on Microwave Photonic*, Oct. 2004, pp. 157–160.

[13] G. Kardaras, T. P. Tien, J. Soler, and L. Dittmann, "Analysis of control and management plane for hybrid fiber radio architectures," in *IEEE International Conference on Communication Technology (ICCT)*, Nanjing, China, November 2010, pp. 281 – 284.

[14] C. I. Cox, E. Ackerman, G. Betts, and J. Prince, "Limits on the performance of RF-over-fiber links and their impact on device design," *IEEE Transactions on Microwave Theory and Techniques*, vol. 54, pp. 906 – 920, 2006.

[15] X. Qi, J. Liu, X. Zhang, and L. Xie, "Fiber dispersion and nonlinearity influences on transmissions of AM and FM data modulation signals in radio-over-fiber system," *IEEE Journal of Quantum Electronics*, vol. 46, pp. 1170–1177, 2010.

[16] X. Gu, Y. He, H. Kosek, and X. Fernando, "Transmission efficiency improvement in microwave fiber-optic link using sub-pico meter optic bandpass filter," in *Proc. of the SPIE Photonic North Conference*, Toronto, Canada, September 2005.

[17] N. Kikuchi, K. Mandai, K. Sekine, and S. Sasaki, "Incoherent 32-level optical multilevel signaling technologies," *Journal of Lightwave Technology*, vol. 26, pp. 150–157, 2008.

[18] N. Kikuchi and S. Sasaki, "Highly sensitive optical multilevel transmission of arbitrary quadrature-amplitude modulation (QAM) signals with direct detection," *Journal of Lightwave Technology*, vol. 28, pp. 123–130, 2010.

[19] S. Yang, T. Lv, G. R. Maunder, and L. Hanzo, "Distributed probabilistic data association based soft reception employing base station cooperation in MIMO-aided multi-user multi-cell systems," *IEEE Transactions on Vehicular Technology*, vol. 60, no. 7, Sept. 2011.

[20] A. Ghosh, R. Ratasuk, B. Mondal, Mangalvedhe, and T. N. Thomas, "LTE-advanced: next-generation wireless broadband technology," *Wireless Communications, IEEE*, vol. 17, pp. 10–22, 2010.

[21] D. Wake, A. Nkansah, and N. J. Gomes, "Radio over fiber link design for next generation wireless systems," *Journal of Lightwave Technology*, vol. 28, pp. 2456–2464, 2010.

[22] G. P. Agrawal, *Nonlinear fiber optics*, Fourth, Ed. Academic Press, 2006.

[23] R. Steele and L. Hanzo, *Mobile Radio Communications*, 2nd ed. IEEE Press - John Wiley, 1999.

[24] G. P. Agrawal, *Fiber Optical Communications Systems*, Third, Ed. John Wiley & Sons, Inc., 2002.

[25] O. Sinkin, J. Holzlohner, R. Zweck, and C. Menyuk, "Optimization of the split-step fourier method in modeling optical-fiber communications systems," *Journal of Lightwave Technology*, vol. 21, pp. 61–68, 2003.

[26] "Spatial channel model for MIMO simulations," Technical specification group radio access network, 2008, ftp://ftp.3gpp.org/.

[27] L. Hanzo, J. Blogh, and S. Ni, *3G, HSDPA, HSUPA and Intelligent FDD versus TDD Networking: Smart Antennas and Adaptive Modulation*. IEEE Press - John Wiley, 2008.

[28] D. Tse and P. Viswanath, *Fundamentals of Wireless Communication*. Cambridge University Press, 2005.
[29] G. Caire, G. Taricco, and E. Biglieri, "Bit-interleaved coded modulation," *IEEE Transactions on Information Theory*, vol. 44, pp. 927–946, May 1998.
[30] L. Hanzo, S. X. Ng, T. Keller, and W. T. Webb, *Quadrature Amplitude Modulation: From Basics to Adaptive Trellis-Coded, Turbo-Equalised and Space-Time Coded OFDM, CDMA and MC-CDMA Systems*. Wiley-IEEE Press, 2004.
[31] J. Hagenauer, "Rate-compatible punctured convolutional codes (RCPC codes) and their applications," *IEEE Transactions on Communications*, vol. 36, pp. 389–400, Apr. 1988.
[32] R. Zhang and L. Hanzo, "Cooperative downlink multicell preprocessing relying on reduced-rate back-haul data exchange," *IEEE Transactions on Vehicular Technology*, vol. 60, pp. 539–545, 2011.

Xinyi Xu received her B.Eng. degree in Electronic Information from Wuhan University, Wuhan, China, in 2004. And She is doing Master of Philosophy towards the degree of Doctor of Philosophy (Ph.D) in the subject area of Communication and Information System at School of Electronic Information in Wuhan University since 2005. In 2008, she was awarded the UK/China scholarships for excellence programme to do Ph.D in the subject area of Radio Communication at School of Electronics and Computer Science, University of Southampton, United Kingdom. Her research interests include optical fibre communication, distributed antennas system, virtual MIMO for Multicell Multiuser networks and radio-over-fibre communications.

Rong Zhang received his B.Eng. degree in communications engineering from Southeast University, Nanjing, China, in 2003 and his M.Sc. degree with distinction in radio frequency communications engineering and Ph.D. degree in wireless communications from the University of Southampton, United Kingdom, in 2005 and 2009, respectively. He was a system engineer with Mobile Communications Division of China Telecom and is currently a research fellow with the Communications Research Group, School of Electronics and Computer Science, University of Southampton. He was awarded a joint EPSRC and Mobile VCE scholarship in 2006. His research interests include cellular networks optimization, multiuser communications, multiantenna communications, and cooperative communications. He is a member of the IEEE and IET.

Salman Ghafoor received the Bachelor of Science (B.Sc) degree in Electrical Engineering from the University of Engineering and Technology (UET), Peshawar, Pakistan in 2006. He received the Master of Science (M.Sc) degree in Electronic Communications and Computer Engineering from the University of Nottingham, UK. Currently, he is a research student at the University of Southampton, UK and is working towards the degree of Doctor of Philosophy (Ph.D). His research interests include optical fibre communication, optical signal processing and radio-over-fibre communications.

Lajos Hanzo FREng, FIEEE, FIET, DSc received his degree in electronics in 1976 and his doctorate in 1983. In 2009 he was awarded the honorary doctorate "Doctor Honaris Causa". During his 35-year career in telecommunications he has held various research and academic posts in Hungary, Germany and the UK. Since 1986 he has been with the School of Electronics and Computer Science, University of Southampton, UK, where he holds the chair in telecommunications. He has co-authored 20 John Wiley - IEEE Press books on mobile radio communications totalling in excess of 10 000 pages, published about 970 research entries at IEEE Xplore, acted as TPC Chair of IEEE conferences, presented keynote lectures and been awarded a number of distinctions. Currently he is directing an academic research team, working on a range of research projects in the field of wireless multimedia communications sponsored by industry, the Engineering and Physical Sciences Research Council (EPSRC) UK, the European IST Programme and the Mobile Virtual Centre of Excellence (VCE), UK. He is an enthusiastic supporter of industrial and academic liaison and he offers a range of industrial courses. He is also a Governor of both the IEEE ComSoc and the VTS. He is the Editor-in-Chief of the IEEE Press and a Chaired Prof. also at Tsinghua University, Beijing. For further information on research in progress and associated publications please refer to http://www-mobile.ecs.soton.ac.uk